Journal of Kyzylorda Scholarly Review

P-ISSN:3006-0265 | E-ISSN:3007-4681. Published by the Open University of Kyzylorda
Copyright © Author(s). This is an open-access article distributed under the terms of the Creative Commons Attribution License (CC-BY).
https://bulletin.ouk.kz/index.php/bulletin/index



# EFFECT OF RESTART VENTING AND PURGE LOSSES ON THE DELIVERABLE HYDROGEN YIELD OF PHOTOVOLTAIC-DRIVEN PEM ELECTROLYSIS PLANTS

**Ghufran Farhan Marzoog**
College of Education for Pure Sciences, University of Wasit, Iraq
*Correspondance: gmarzoog@uowasit.edu.iq

**Article History:**
Received: 30th Sept 2026; Revised: 20th Oct 2026; Accepted: 10th Nov 2026; Published: 22th Nov 2026

**Abstract:** Photovoltaic (PV) electrolysis plants using a proton exchange membrane (PEM) shut down nearly daily. Models account for a constant efficiency when purifying the gas and treat start-up as a delay. Any hydrogen that is vented, purged, or diverted during a restart will not be accounted for in these models. An event-based model was developed to track the fate of stack hydrogen and determine how much of it a restart withholds from delivery. The model was applied to measured minute resolution solar irradiance for a MW scale PEM plant in three climates. If the plant depressurized and purged with nitrogen at each stop, restarts withheld 2-15 % of stack hydrogen from delivery. It was determined that the daily stop, not intra-day cycling, set this loss. Using a steady purification model caused an overestimate of delivered hydrogen by 3-37 % under the same practice. Hourly input concealed restart attempts that minute data resolved. Hot standby avoided most of the modeled loss but, at the standby power measured on a working plant, raised the energy spent per kilogram delivered. Gas inventory dominated the uncertainty. More information about the gas stored in a PEM plant will need to be obtained to decrease the uncertainty in the model. Since the loss drivers rest on component-level tests rather than plant measurements, measured inventories and per-restart hydrogen balances are the first data needed to confirm these results.

**Keywords**: Gas purification, Hot standby, Start-up, Temporal resolution, Uncertainty quantification

## Introduction

Solar irradiance that is fed to a photovoltaic (PV) electrolysis plant is variable. With a direct coupling to PV the electrolyzer will need to shut down many times a day [1]. The amount of hydrogen that can leave the plant, not the hydrogen formed in the stack, is what needs to be considered. There are different purity grades of hydrogen that need to be met. One example would be the Grade D limits of ISO 14687, which has purity levels that need to be achieved [2]. A critical review of the literature that discusses the dynamic behavior of PEM electrolysis shows that not many papers cover the full system [3].

Models have tried to represent the dynamics of the stack in several ways, and each family leaves a different part of the restart unaccounted for. Some have added a hot or cold start up

to their model [4] or looked into how cooling down an electrolyzer affects its performance [5]. Others have used 5-minute resolution to represent solar irradiance [6]. Research has been done to see if cold starts of an electrolyzer can be shortened through power or current control [7], [8] and how to best get the stack up to temperature [9]. All of these studies will show that start up takes away from production either in time or energy. There are also studies that have looked at different resolutions and found that sub-hourly input changes the predicted yield and number of times the system is on and off [10] and hydrogen output under variable efficiency [11]. It also changes reconfiguration events [12] and cost [13], [14].

They mostly leave out purification. There is one model with purification included which assumes a constant load dependent purge loss [15] and a balance of plant model that considers purge and dryer regeneration losses [16]. There are also component level studies of dryer recovery and purge demand [17], [18], [19] as well as deoxo performance [20], [21], [22]. Other studies focus on crossover during low loads [23], [24], [25] or when transitioning between states.

Plant records nevertheless describe hydrogen produced without delivery. Examples are pressurization without product flow [26], losses of purged gas during operation of a PV powered hydrogen pilot plant [27] and off-specification gas during cold starts [7]. Data has been collected from start ups [28], [29], [30] and there is a model of a MW scale plant [31]. But none that were found calculate how much of the purged and vented hydrogen can be attributed to each restart and therefore the annual deliverable compliant yield at a minute time step.

This work aims to fill this gap using an event based model for each restart using measured 1 minute irradiance data. How much stack hydrogen is withheld from delivery during a restart and what contributes to it? How does using conventional yield models with hourly inputs over or underestimate the delivered hydrogen? What variables will have the largest impact on this and can stop policies affect it? The results show that the daily depressurizing stop drives the amount of hydrogen lost and that the gas inventory is the largest source of uncertainty.

The three contributions are, first, an event based model with hydrogen fate accounting, verified numerically and exposed to component level tests reported in full. Second, how much hydrogen is lost from a restart and the deliverable hydrogen yield for a PV powered PEM plant are quantified by mechanism, event class, site, and stop policy, with a global uncertainty analysis. Third, the bias from modeling purification as a steady process is separated from the bias from using hourly inputs, and the standby trade-off is stated. Section II will discuss related work, Section III explains the methods, Section IV talks about the findings and Section V states the scope of the study. Section VI is a conclusion.

**Related Works**

The five recent works that frame this study are compared to this work in Section IV-J. Steady purification models include one by Renau et al. [15] who used a polynomial PEM model and hourly solar data. They implemented a purge loss from pressure swing adsorption (PSA) which falls steeply with load. Restart events were not accounted for. There are two papers that looked into shortening the cold start of alkaline water electrolysis (AWE). Xu et al. [8] did this by implementing a startup aware control strategy for multiple stacks. And Dong et al. [7] implemented self-heating and auxiliary heating on a 250 kW system. Dong et al. [7] stated they vented off-specification gas but did not say how much. No mention of purification was found in either paper. Two papers dealt with variability of the input. Virah-Sawmy et al. [11] showed that assuming a constant efficiency will over predict hydrogen more than using a coarser timestep does. They included start up as a loss for 5 minutes. Almpantis et al. [12] showed an over prediction of hydrogen and lower number of reconfigurations when using hourly data on a small stack during the summertime. None of the five papers reports a deliverable hydrogen yield per restart.

Journal of Kyzylorda Scholarly Review
P-ISSN:3006-0265 | E-ISSN:3007-4681
https://bulletin.ouk.kz/index.php/bulletin/index

## Materials and Method

### A. Plant, Delivery Criterion, And Stop Policies

The modeled plant couples 1.5 MWp of fixed-tilt photovoltaics on the direct-current (DC) side to a 1 MW PEM electrolyzer, treated as one restart unit (Fig. 1). This sizing lies inside the PV-to-electrolyzer range of 1.4-2 reported by Renau et al. [15], and power above the rated stack power is clipped. Product gas passes a separator and cooler, a palladium deoxo unit, and an adsorption dryer before the delivery point. Hydrogen counts as delivered only if it meets the Grade D limits of ISO 14687:2025: H2O ≤ 5, O2 ≤ 5, N2 ≤ 300, and total non-hydrogen gases ≤ 300 µmol/mol [2]. Auxiliaries and standby power come from an auxiliary supply, because the main metric is defined on stack hydrogen; drawing the balance of plant (BoP) from the PV bus is reported as a sensitivity. Table I lists the parameters and their sources.

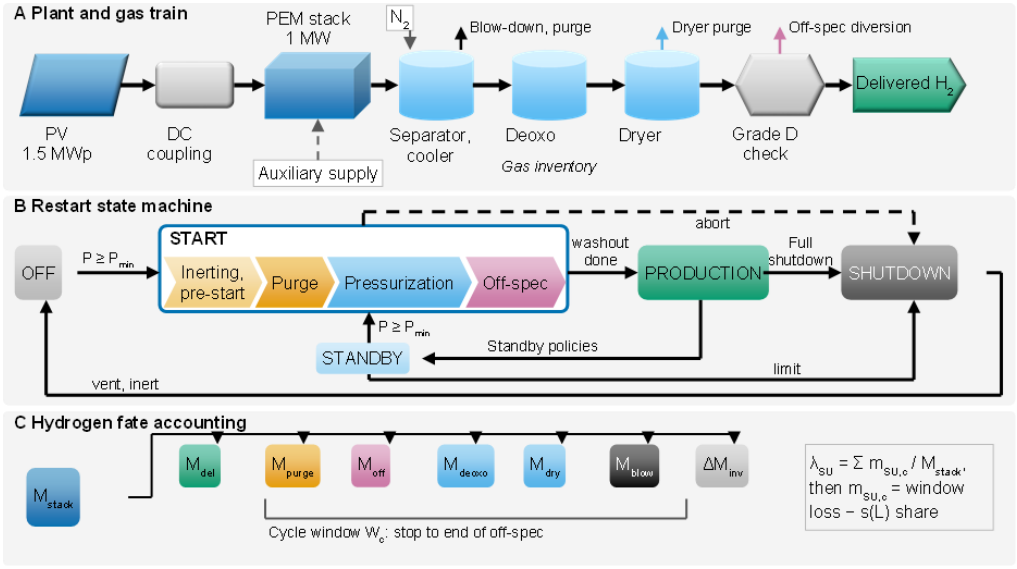


**Figure 1.** Plant layout, restart state machine, and hydrogen fate accounting (conceptual schematic, no measured data). (A) Gas train with vent paths. (B) Plant states and transitions. (C) Fates of stack hydrogen and the restart window.

Four stop policies span the documented practices. A fifth case is presented that bounds them. Full shutdown means that all pressure is drained and the plant is inerted at every stop. This is what was done on the PV system [27]. Time-limited standby holds hot standby for up to 15, 30, 60, or 120 min and then shuts down in the same way. Daytime standby holds standby through daylight stops and shuts down overnight. The 24-h standby policy holds hot standby for up to 24 hours before shutting down. This was implemented on a 250 kW plant [26]. The pressure-hold bound retains the inventory at zero standby power while the stack cools. There is no decay of pressure, no handling of crossover, and no source. This was added only to attribute the increase in hydrogen from 24-h standby to retained inventory or retained heat.

### B. Irradiance Data And Pv Chain

Irradiance data from 1-min global direct and diffuse measurements of Baseline Surface Radiation Network [32] at Cabauw, Carpentras and Gobabeb which exhibit varying levels of intermittency (Table II) were used. Years that could be considered ranged from 2013-2018 as these years exist in all 3 data sets. If at least 95% of the daytime minutes of a year (zenith angle below 85 degrees) held all three components within the physical and closure limits defined by Long and Shi [34] the year was used. This resulted in 17 site years which were all included. Missing values were first replaced using closure for global irradiance and decomposition of Erbs et al. [35] for direct and diffuse. Linear interpolation was then applied to the remaining values using the clear sky index [33]. When values are given for three sites they will be listed in this order.

Journal of Kyzylorda Scholarly Review
P-ISSN:3006-0265 | E-ISSN:3007-4681
https://bulletin.ouk.kz/index.php/bulletin/index

Transposition of plane of array irradiance was done using the method of Perez et al. [37] and panels were oriented towards the equator at the median PVGIS optimum tilt angle. A nominal operating cell temperature of 45°C was used along with a DC model from Dobos [38]. A temperature coefficient of −0.47%/°C and 14% loss was applied to system output. Albedo was set to 0.2 and DC/DC efficiency was 1. There were no losses due to incidence angle, and the effects of the previous two are explored in section 4.9. Albedo was not explored. PVGIS data at hourly time steps [36] was obtained at each coordinates and year used for one baseline only.

**C. Restart State Machine**

A state machine advances on a 1-min grid through OFF, STANDBY, START, PRODUCTION, and SHUTDOWN (Fig. 1B). Stops, restart attempts, and aborts follow the minimum load $P_{min}$ with a debounce time $t_{deb}$. After a depressurized stop, START runs inerting and pre-start without production, a purge with product vented, pressurization into the gas inventory, and off-specification diversion. Nitrogen washout ends when purged and diverted gas together reach $\theta_{spec}$, expressed in rated-minutes, where one rated-minute is the hydrogen produced in 1 min at the rated flow $\dot{m}_r$ = 0.336 kg/min. The value of $\theta_{spec}$ assumes that the purge of the pilot plant ends at specification, although that purge runs on a fixed time without a composition criterion [27]. PRODUCTION then delivers stack hydrogen minus the steady dryer share and the deoxo demand.

When an abort occurs SHUTDOWN is entered into for full shutdown or STANDBY for the rest. Once standby limit is reached SHUTDOWN is entered into. At SHUTDOWN all inventory is vented and takes 20 minutes on the 1 minute timestep. From standby there is no additional loss as pressure and temperature are maintained when full. Standby does not incur hydrogen losses. All years begin in OFF mode and are cold and have no pressure at 00:00 UTC which is roughly 20-60 minutes after solar midnight.

Thermal behavior rests on measured durations, not on a heat-up simulation. The stack power cap rises linearly from zero to rated power over a start-up time taken from the anchors measured on a 190 Nm³/h PEM system [28]. Linear interpolation in the initial temperature fills the span between them, and restarts from STANDBY use the hot value. An idle stack cools by a lumped model with the thermal capacity and resistance of Rauls et al. [9]. Restarts are classed hot (from STANDBY), warm (from OFF with at least half of the temperature excess retained), or cold.

**D. Hydrogen Accounting And Metrics**

Annual stack hydrogen $M_{stack}$ after Faradaic efficiency closes on the fate balance

$$M_{stack} = M_{del} + M_{purge} + M_{off} + M_{deoxo} + M_{dry} + M_{blow} + \Delta M_{inv} \quad (1)$$

with delivered, purge, off-specification, deoxo, dryer, and blow-down masses and the inventory change over the year. A cycle $c$ is a stop plus the following restart. Its window $W_c$ opens at stop entry and closes at the end of off-specification diversion, and its excess loss is

$$m_{SU,c} = \sum_{k \in W_c} \left( m_{purge,k} + m_{off,k} + m_{deoxo,k} + m_{dry,k} + m_{blow,k} \right) - \sum_{k \in W_c} m_{stack,k}\, s(L_k) \quad (2)$$

where the second sum is the steady dryer loss that the same power trajectory would carry at load $L$. Only the excess over steady operation therefore counts as a restart cost, and for this reason a window can be slightly negative under standby policies. The main metric, the restart

Journal of Kyzylorda Scholarly Review
P-ISSN:3006-0265 | E-ISSN:3007-4681
https://bulletin.ouk.kz/index.php/bulletin/index

loss in percent of stack hydrogen, is

$$\lambda_{SU} = 100\,\frac{\sum_c m_{SU,c}}{M_{stack}} \quad (3)$$

Production forgone during START delays is excluded from $\lambda_{SU}$ and appears in delivered mass. The first cycle of each year is counted in $\lambda_{SU}$, with an effect of at most 0.029 percentage points (pp) under full shutdown and 0.020 pp under daytime standby.

The remaining metrics follow from these terms. The equivalent restart time $\tau_{eq,c} = m_{SU,c}/\dot{m}_r$ expresses a cycle in rated-minutes, and its mean per completed restart is $\bar{\tau} = \lambda_{SU} M_{stack}/(100\,N_c\,\dot{m}_r)$, with $N_c$ completed restarts per year and aborted attempts in the numerator. Deliverable efficiency is $\eta_{del} = M_{del}/M_{stack}$, and delivered specific energy $SEC_{del}$ is stack, BoP, and standby energy over $M_{del}$ [39]. The bias of a baseline $b$, $\beta_b = 100\,(M_{del,b} - M_{del})/M_{del}$, is positive when the baseline overestimates delivered hydrogen.

**E. Stack, Gas, And Purification Submodels**

Cell voltage uses Nernst + Tafel terms along with an ohmic term based on membrane conductivity [40], scaled once to the rated point [9]. Faradaic efficiency uses Persson et al. [26]. This leads to a stack specific energy of roughly 50 kWh/kg.

The inventory filled in pressurization and vented at blow-down is $m_{full} = i\,\dot{m}_r\,(p_{op} - p_0)$, with normalized inventory $i$ in minutes of rated production per bar, operating pressure $p_{op}$, and $p_0$ = 1.013 bar. The nominal $i$ derives from about 1.7 kg of hydrogen equivalent pressurized in 45 min at 82-143 kW on a 250 kW plant to about 30 bar, a pressure inferred by the source [26]. This gives 6.80 kg at nominal conditions. The lower end of its range derives from the statement that a 100 kW PEM system takes roughly 5 min to pressurize and start [29].

The steady dryer share is $s(L) = \phi + b/\max(L, 0.10)$, a constant purge flow term plus a throughput term, calibrated at 10 % and 100 % load of the table of Renau et al. [15]. Deoxo consumes 2 H2 per O2 at an oxygen level from a steady power-law fit to Liu et al. [30]. Because a Pd/Al2O3 deoxo catalyst removed up to 99.99 % of oxygen in laboratory tests [21], this stoichiometric form states the hydrogen demand, not the transient; catalyst light-off is not represented.

Dryer regeneration state lies outside the plant model and outside $\lambda_{SU}$. A one-dimensional bed model of the vacuum pressure swing adsorption dryer of Santos et al. [19] instead gives per-restart bounds. It uses the published isotherms, a water mass-transfer coefficient calibrated on one breakthrough curve and frozen before held-out tests, a regeneration form that allows high water fractions, and the published scale-up rule at the plant rated flow.

A mechanism counts as influential when switching it off changes $\lambda_{SU}$ by at least 0.1 pp at one or more sites. For full shutdown, where each completed restart repeats one blow-down and one washout, the accounting also suggests a closed-form estimator:

$$\hat{\lambda}_{SU} = 100\,\frac{N_c\,\dot{m}_r\left[i\,(p_{op} - p_0) + \theta_{spec}\right]}{M_{stack}} \quad (4)$$

**Table 1.** Main Parameters, Sampled Ranges, and Sources

| Parameter | Nominal | Sampled range | Source |
|---|---|---|---|
| Rated point | 1.75 A/cm², 1.80 V, 75 °C | fixed | Rauls et al. [9] |
| PV-to- | 1.5 | 1.0-2.0, | Renau et al. [15] |

Journal of Kyzylorda Scholarly Review
P-ISSN:3006-0265 | E-ISSN:3007-4681
https://bulletin.ouk.kz/index.php/bulletin/index

| Parameter | Nominal | Sampled range | Source |
|---|---|---|---|
| electrolyzer ratio | | sensitivity indices only | |
| Minimum load $P_{\min}$ | 0.10 $P_{\text{rated}}$ | 0.10-0.191 $P_{\text{rated}}$ | Virah-Sawmy et al. [11]; Renau et al. [15] |
| Standby power | 0.095 $P_{\text{rated}}$ (midpoint) | 0.01-0.18 $P_{\text{rated}}$ | Virah-Sawmy et al. [11]; Persson et al. [26] |
| Inventory $i$ | 0.699 min/bar | 0.120-0.888 min/bar | Flamm et al. [29]; Persson et al. [26] |
| Operating pressure $p_{\text{op}}$ | 30 bar | 15.8-30 bar | Aijun et al. [28]; Persson et al. [26] |
| Washout $\theta_{\text{spec}}$ | 6.5 rated-minutes | fixed | Bonaccorsi et al. [27] |
| Inerting, pre-start, final inerting | 7, 1, 8 min | fixed | Bonaccorsi et al. [27] |
| Purge time | 6.5 min | 6-7 min | Bonaccorsi et al. [27] |
| Depressurization time | 11.2 min | 3-16 min | Bonaccorsi et al. [27] |
| Cold start | 6340 s from 26 °C | 2040-6340 s | Liu et al. [30]; Aijun et al. [28] |
| Hot start | 1100 s from 63.5 °C | fixed | Aijun et al. [28] |
| Thermal capacity | 4408 kJ/K per MW | 1024-5377 kJ/K per MW | Rauls et al. [9]; Pfennig et al. [31], model-derived |
| Thermal resistance | 2.3 K/kW | 2.3-10.5 K/kW | Rauls et al. [9]; Pfennig et al. [31], model-derived |
| O2 in H2 at deoxo inlet | 9.54 ppm at 1 A/cm², exponent 0.658 | 5.86-2500 ppm | Liu et al. [30]; Aijun et al. [28] |
| Steady dryer share | $\phi$ = 0.0137, $b$ = 0.0253 | fixed | Renau et al. [15] |
| Debounce time $t_{\text{deb}}$ | 1 min | fixed | Design choice |

Note: $\mathrm{P}_{\text{rated}}$ is the rated stack power. Ranges are uniform on sourced bounds; ends derived from alkaline sources enter only as scenarios (Section IV-I). Scenario values are listed in Table II.

### F. Baselines

All baselines were re-run on the same inputs, and the proposed formulation is called the event model where a contrast is needed. The fixed-efficiency model is the classical approach: 75 % stack efficiency on the lower heating value (LHV), constant recovery of 98.4 %, the product recovery reported for the deoxo and adsorption dryer of an alkaline system [41], a $P_{min}$ cut-off, and no start-up loss. The hourly feasibility model represents feasibility-study practice: hourly PVGIS data, a constant net consumption of 67 kWh/kg [17], and a $P_{min}$ cut-off. The steady-purge model is the class of Renau et al. [15]: the steady loss $s(L)$ with instant switching. The efficiency-curve model re-runs Virah-Sawmy et al. [11]. Its three curves fall from 0.75 at 0.3 $P_{cap}$ to 0.70, 0.60, and 0.55 at $P_{cap}$, with a $P_{min}$ of 0.1 $P_{cap}$, standby of 0.01 $P_{cap}$, a 5-min start-up energy penalty, and no purification. Dispatch is solved by dynamic programming with perfect foresight. The start-up-delay model stands for dynamic start-up models without purification: the thermal ramp and switching events remain, whereas purification mechanisms are off. The controllers of Xu et al. [8] and Dong et al. [7] were not re-implemented.

Two ordered chains decompose the bias, each taking one step at a time away from the base case towards the event model. For the fixed-efficiency model this includes the efficiency convention, dispatch, steady purification model, start up delays and losses due to starting up purification. The two biggest steps were also reversed. The chain of the hourly feasibility model included the irradiance source, resolution, consumption convention with steady purification and start up delays and losses.

### G. Verification and Component-Level Tests

Gap filling, tolerances, classification rules, decomposition orders, and the estimator of (4) were fixed before any annual run. The tolerances are an absolute relative error of 20 % for scalar quantities, a normalized root-mean-square error of 15 % for time series, and 0.15 in absolute log10 difference for impurity levels. Calibration and held-out roles were also assigned before fitting, and a test outside tolerance led to wider uncertainty ranges, not to tuning on held-out data.

Numerical verification comprised annual closure at $10^{-6}$ relative or better, limiting cases, analytic washout and inventory checks at 0.1 %, and a 10 s versus 1 min step comparison. Published numbers of Virah-Sawmy et al. [11] were re-run on the public 2022 market data of the Australian National Electricity Market within 10 %, and a link test tied the plant accounting to that re-run with zero difference. The dryer bed model was checked against a reference solution for grid and tolerance convergence and against a second, finite-element solver, and the PV chain was compared with PVGIS output.

Submodels have been compared to data at component level. Time to heat up is from a PEM system [9]. Time to pressurize is from the alkaline pilot [27] and a 100 kW PEM system [29]. Oxygen content in hydrogen has been compared to current [28], [30], the steady purge share has been compared to load [15]. Dryer breakthrough and partial regeneration were tested without calibration [19].

### H. Uncertainty, Sensitivity, And Scenarios

Ten epistemic factors of Table I were sampled uniformly on sourced bounds with a scrambled Sobol sequence of 1024 points and five seeds. All 17 site-years ran under four policies (full shutdown, 60-min standby, daytime standby, and 24-h standby), 348 160 annual runs in total. Before the final runs, the ranges were restricted to PEM evidence; the pressure range therefore starts at 15.8 bar, because 12 bar is an alkaline threshold. Each interval pools all site-years of a site with equal year weight, and percentiles are taken per seed and averaged over seeds. A 90 % interval here is the 5th to 95th percentile span of the sampled ranges, not a probability for a real plant. Every $\lambda_{SU}$ interval holds within the modeled mechanisms, with dryer regeneration state excluded, washout fixed at its nominal value, and a PV ratio of 1.5, since PV sizing is a design factor and not an epistemic one.

Journal of Kyzylorda Scholarly Review
P-ISSN:3006-0265 | E-ISSN:3007-4681
https://bulletin.ouk.kz/index.php/bulletin/index

A materiality rule classes each site and policy: material when the 5th percentile of $\lambda_{SU}$ is at least 1.0 %, negligible when the 95th percentile is below 0.5 %, and condition-dependent otherwise. The 1 % level is the order of the modeling biases that Virah-Sawmy et al. [11] and Almpantis et al. [12] report as consequential.

Sobol indices used Saltelli sampling with $N = 1024$ (13 312 rows per seed), five seeds, and 1000 bootstrap resamples. They cover full shutdown, 60-min standby, and daytime standby at one reference year per site, chosen in advance, with PV sizing as an eleventh factor labeled design. The pooled five-seed estimator is the one reported, because its largest half-width is 0.028 over 26 estimates with total index at least 0.1, whereas single-seed half-widths exceed 0.05 in 40 of 130 estimates. Bootstrap on a scrambled sequence overstates the spread, since the seed standard deviation of the total index stays at or below 0.0062. Percentiles varied across seeds by at most 1 % of their mean or 0.01 pp in 36 of 36 checks. The estimator reproduced the Ishigami function with a five-seed mean error of 0.0097, although 2 of 30 single-seed estimates exceeded 0.02. No significance test was applied, because the outputs are deterministic; the descriptive slope in Section IV-D carries a confidence interval clustered by site-year.

Three further studies complete the design. The resolution study replaces the 1-min series by block means and adds a 2 × 2 factorial on input (1, 60 min) and model (event, steady-purge). A deterministic grid under full shutdown and daytime standby tests the conditions of the conclusion (Table II). Removing the cycles that touch a filled minute, which make up 7.8, 2.9, and 6.3 % of full-shutdown cycles, lowered nominal $\lambda_{SU}$ by 1.2, 0.3, and 0.4 pp and moved the median equivalent restart time by at most 0.07 rated-minutes.

**Table 2.** Sites and scenarios

| Item | Setting |
|---|---|
| Cabauw | 51.968° N, 4.928° E; temperate maritime; 6 site-years, 2013-2018; tilt 40°; DC capacity factor 12.0 % |
| Carpentras | 44.083° N, 5.059° E; Mediterranean; 5 site-years, 2014-2018; tilt 39°; DC capacity factor 17.0 % |
| Gobabeb | 23.561° S, 15.042° E; hyper-arid; 6 site-years, 2013-2018; tilt 25°; DC capacity factor 22.5 % |
| Input resolution | Block means of 5, 15, 30, and 60 min held on the 1-min grid |
| Controller | Debounce time of 5 and 15 min; abort-hold variant |
| PV sizing | PV-to-electrolyzer ratios of 1.0 and 2.0, one seed, no class assigned |
| Steady dryer term | Constant shares of 1.02 % [19] and 1.6 % [41] |
| Deterministic grid | Washout {0, 1, 2, 3.25, 6.5, 13, 25, 50, 100} rated-minutes × inventory {0.120, 0.699} min/bar × pressure {12, 15.8, 30} bar, full shutdown and daytime standby |

Note: DC capacity factor is the mean DC power over the PV peak.

Journal of Kyzylorda Scholarly Review
P-ISSN:3006-0265 | E-ISSN:3007-4681
https://bulletin.ouk.kz/index.php/bulletin/index

## Results and Discussion

### A. Verification Holds, Whereas Component Tests Leave The Loss Drivers Open

The plant model met every numerical verification check, whereas the component-level tests left the two loss drivers untested or outside tolerance (Fig. 2). Hydrogen closure reached 5.6 × $10^{-12}$ and energy closure 7.8 × $10^{-13}$ over all stochastic runs, and the step comparison changed λ_SU by 0.09 %. All 12 re-run values of Virah-Sawmy et al. [11] fell within 10 %, with a largest deviation of 5.2 %; this re-run covers dispatch, aggregation, and accounting, but it does not test the polarization model or the restart states. It took the place of the known cases of Rauls et al. [9] and Persson et al. [26], which could not be reproduced from the printed information. The dryer reference bed met 70 of 91 grid and tolerance checks, and the regeneration form outside them was replaced. The second solver agreed in 28 of 28 verification cases and reproduced the dryer outlet water fraction within 0.10-0.23 %, which is an implementation check only, and annual PV energy differed from PVGIS output by −3.3 to +8.7 %.

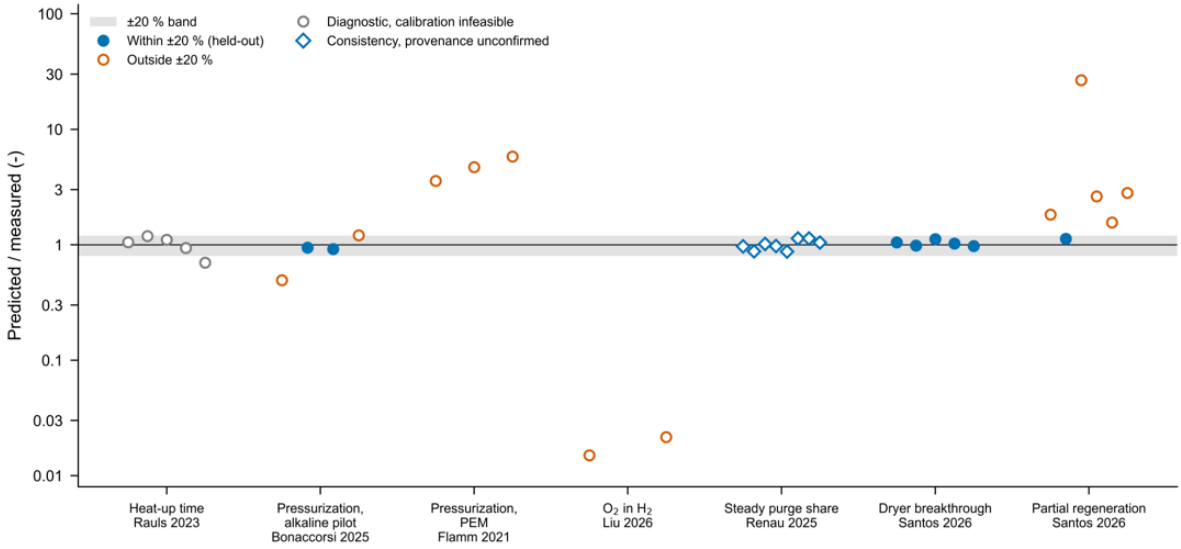


**Figure 2.** Ratio of predicted to measured values in the component-level tests. The gray band marks ±20 %. Filled circles are held-out points within the band, open circles lie outside it, gray circles are diagnostics of a test whose calibration was infeasible, and diamonds mark a consistency check on a source table of unconfirmed provenance.

Only the steady purge share which had uncertain data provenance and dryer breakthrough stayed within the acceptable range. Thermal start-up could not be calibrated as the loss-free bound of 81.0 min was above the 77 min target. Two out of 4 points from the alkaline pilot were within the acceptable range when pressurizing. The only independent PEM pressurization datum implies an inventory 3.6-5.8 times below the nominal, and that test was run with foreknowledge of its likely direction. Nitrogen washout could not be tested, for the reason given in Section III-C. The oxygen test compared a steady law with a transient peak, which was outside of the acceptable range. Partial dryer regeneration fell outside the acceptable range without any calibration. The dryer recovery chain was not executed due to missing source data and deoxo start-up did not need to be tested as its ablation stayed at or below 0.001 pp.

### B. Blow-Down and Washout Set The Cost Of Each Restart

A complete shutdown will cost one blow-down and one washout to start back up and this amount will be independent of temperature (Fig. 3). Panels A-C show the course of one day with the median production from the stack out of 137 days in 2013 at Cabauw where there was at least one completed start up and one aborted. There were two aborted starts up in the

Journal of Kyzylorda Scholarly Review
P-ISSN:3006-0265 | E-ISSN:3007-4681
https://bulletin.ouk.kz/index.php/bulletin/index

morning venting a partial inventory before a completed one started up, so that the stack produced 53.7 kg while the plant delivered 39.8 kg.

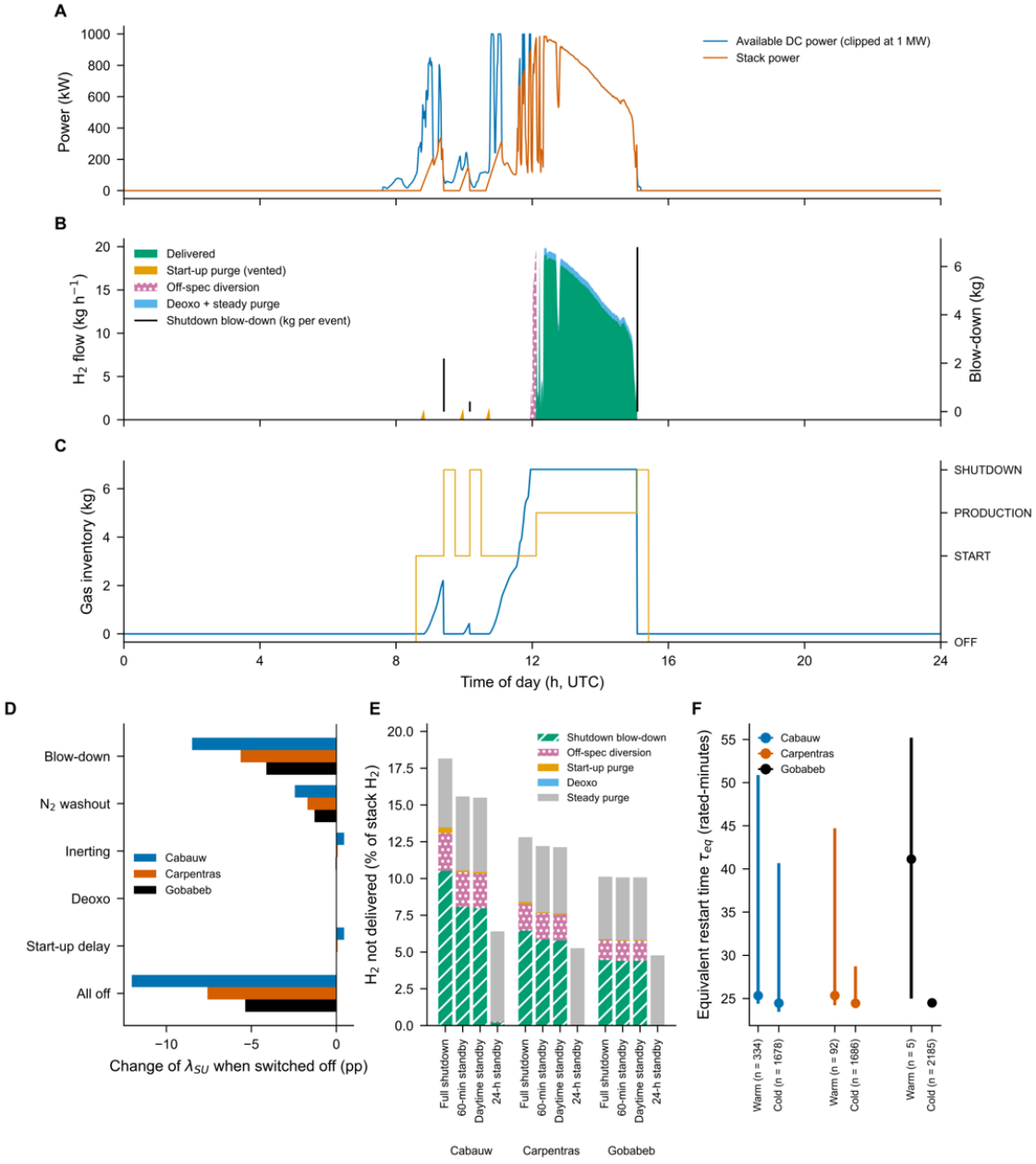


**Figure 3.** Hydrogen fate at restart under the stop policies. (A-C) One restart day at Cabauw in 2013 under full shutdown: (A) available DC power and stack power, (B) hydrogen flows by fate, with blow-down masses per event on the right axis, and (C) gas inventory and plant state. (D) Change of λ_SU when one mechanism is switched off, full shutdown. (E) Hydrogen not delivered by mechanism and policy at nominal parameters. (F) τ_eq by thermal class under full shutdown; dots are medians, lines span the 10th to 90th percentile, and tick labels give the number of cycles.

The arithmetic of a nominal cycle explains the median equivalent restart time of about 24.5 rated-minutes at all three sites. The inventory of 6.80 kg equals about 20 rated-minutes, washout adds 6.5, and the steady reference removes the rest. Single-mechanism ablation assigns 71-77 % of the modeled λ_SU to blow-down and 20-24 % to nitrogen washout with off-specification diversion (Fig. 3D), together more than 90 %. Stoichiometric deoxo, in

contrast, stays at or below 0.001 pp even at 2500 ppm of oxygen, so it is non-influential within that representation. Removing inerting raises the loss by up to 0.45 pp, because a shorter START exposes more partial pressurizations to aborts, and the sum of single ablations differs from the all-off case by at most 1.56 pp. Across policies, blow-down shrinks as fewer stops depressurize, while the steady purge share persists (Fig. 3E).

No trend of cold greater than warm greater than hot was found (Fig. 3F). Warm restarts had a median of 25.3 rated-minutes at both Cabauw and Carpentras compared to 24.5 for cold, since there is no temperature dependence of the blow-down and washout and returns from hot standby carry no excess by construction. There were only 5 cycles at Gobabeb for the warm median to be calculated from so it can only serve as an indication.

**C. Restart Loss Is Material Wherever The Plant Still Vents**

Full shutdown, 60 min standby and daytime standby all showed a material restart loss at the three sites within the modeled mechanisms (Table III). There will be a similar amount of mass lost to start up every year under full shutdown regardless of location (3.0-3.3 t yr-1) since about one blow-down and washout recur per day. This leaves the difference between locations coming from their production from the stack over a year (27.6, 41.4 and 56.3 t yr-1) and will scale with blow-down and washout / production from the stack. Having a standby will reduce the average amount of mass lost to start up at Cabauw but not at Gobabeb due to more stops occurring during the night. When comparing PV ratios with no class the lowest 5th percentile for the 3 policies was 1.71 % with a ratio of 2.0.

**Table 3.** Restart loss λ_SU, mean equivalent restart time τ ¯, and deliverable efficiency η_del by site and stop policy, with i the normalized inventory. Intervals follow Section III-H

| Site | Policy | $\lambda_{SU}$ nominal (%) | $\lambda_{SU}$ at $i$ = 0.120, 30 bar (%) | $\lambda_{SU}$ P5/P50/P95 (%) | $\bar{\tau}$ P5-P95 (rated-minutes) | $\eta_{del}$ P50 | Class |
|---|---|---|---|---|---|---|---|
| Cabauw | Full shutdown | 12.03 | 5.17 | 5.94/9.94/15.28 | 10.8-32.3 | 0.841 | Material |
| Cabauw | 60-min standby | 9.34 | 3.47 | 3.56/6.19/9.79 | 2.2-8.1 | 0.877 | Material |
| Cabauw | Daytime standby | 9.25 | 3.40 | 3.42/6.02/9.58 | 2.1-7.6 | 0.879 | Material |
| Cabauw | 24-h standby | 0.248 | 0.093 | 0.120/0.247/0.501 | 0.058-0.203 | 0.936 | Condition-dependent |
| Carpentras | Full shutdown | 7.58 | 2.96 | 3.27/5.54/8.57 | 9.8-28.1 | 0.892 | Material |
| Carpentras | 60-min standby | 6.93 | 2.53 | 2.56/4.49/7.16 | 4.1-13.5 | 0.902 | Material |
| Carpentras | Daytime standby | 6.86 | 2.48 | 2.49/4.40/7.03 | 3.9-12.8 | 0.903 | Material |
| Carpentras | 24-h standby | 0.045 | 0.019 | 0.012/0.061/0.170 | 0.016-0.175 | 0.946 | Negligible |
| Gobabeb | Full shutdown | 5.36 | 1.93 | 1.99/3.50/5.60 | 8.9-25.3 | 0.916 | Material |
| Gobabeb | 60-min standby | 5.29 | 1.89 | 1.90/3.38/5.43 | 7.2-21.0 | 0.917 | Material |
| Gobabe | Daytime | 5.29 | 1.89 | 1.90/3.38/5.43 | 7.2-20.9 | 0.917 | Material |

Journal of Kyzylorda Scholarly Review
P-ISSN:3006-0265 | E-ISSN:3007-4681
https://bulletin.ouk.kz/index.php/bulletin/index

| Site | Policy | $\lambda_{SU}$ nominal (%) | $\lambda_{SU}$ at $i$ = 0.120, 30 bar (%) | $\lambda_{SU}$ P5/P50/P95 (%) | $\bar{\tau}$ P5-P95 (rated-minutes) | $\eta_{del}$ P50 | Class |
|---|---|---|---|---|---|---|---|
| b | standby | | | | | | |
| Gobabeb | 24-h standby | 0.00236 | 0.00308 | 0.00244/0.00289/0.00323 | 0.007-0.010 | 0.950 | Negligible |

Note: Nominal values are means over site-years; P5, P50, and P95 are the 5th, 50th, and 95th percentiles. The mean τ ¯ is shown because the median τ_eq is 0 wherever returns from hot standby, which carry no excess, form more than half of the completed restarts.

The nominal values are not central. Nominal λ_SU lies at the 74th-94th percentile of the ensemble under the three venting policies, and at the 50th, 38th, and 3rd percentile under 24-h standby, so the classes rest on the pooled intervals.

Under 24 h standby the class is negligible at Carpentras and Gobabeb and condition-dependent at Cabauw, with a 95th percentile that is 0.0008 pp over the threshold, which is less than the spread between seeds of 0.0024 pp. Neither class means a material loss. The residual comes from stops that last longer than the 24 h limit, with 53, 11 and 0 cycles of about 8 kg each and the shortest lasting 25.9 and 41.6 h. The first cycle of each simulated year accounts for 1.9, 7.4 and 100 % of the nominal value.

**D. The Daily Depressurized Stop Sets The Loss**

Daily loss is roughly constant and therefore the increase in the daily ratio with intra-day attempts comes from less production daily (Fig. 4). This ratio increases from 7.1 % for days with no intra-day attempts to 35.7 % on the most intermittent days at Cabauw. The loss remained 8 to 11 kg/day or 24-34 rated-minutes on days with up to three intra-day attempts at all sites and up to 8 at Cabauw. It did not increase beyond this on days with more intermittent operation. Stack production decreased by a factor of up to about 4 across these bins. The first extra attempts at Cabauw increased the daily loss by around 1 kg each.

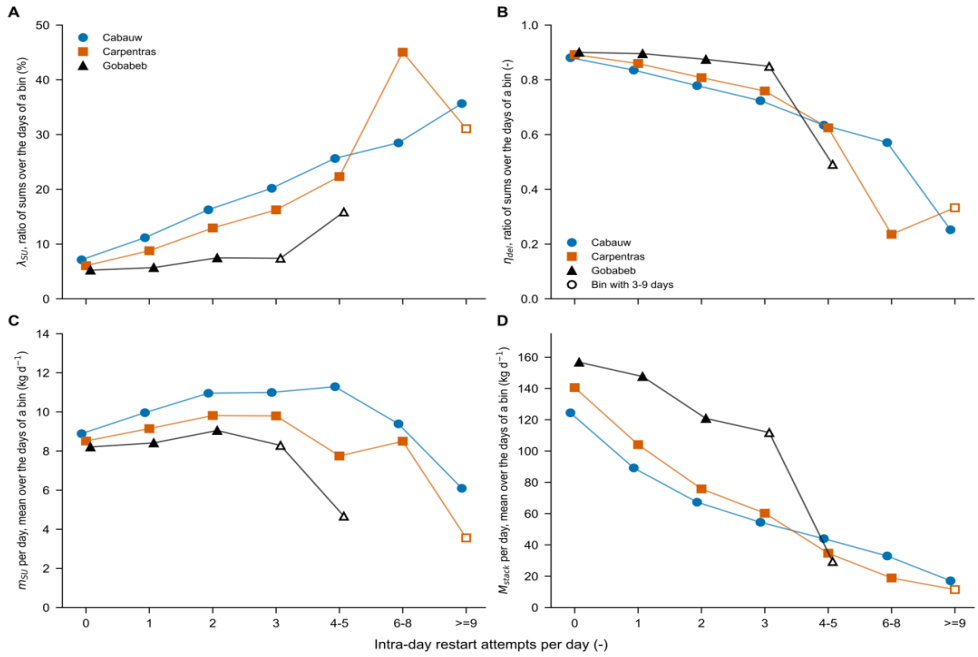


**Figure 4.** Daily statistics under full shutdown by intra-day restart attempts. (A) λ_SU and (B) η_del as ratios of sums. (C) Mean m_SU and (D) mean M_stack per day. Bins with fewer than 3 days are omitted; open markers denote 3-9 days.

Journal of Kyzylorda Scholarly Review
P-ISSN:3006-0265 | E-ISSN:3007-4681
https://bulletin.ouk.kz/index.php/bulletin/index

A descriptive slope gave 4.81 ± 0.59, 6.47 ± 0.66, and 1.20 ± 0.50 pp per intra-day attempt ($R^2$ 0.21, 0.29, and 0.13; site-year clustered 95 % interval). It describes an association with a small denominator, not a cost per attempt. Completed restarts numbered 335, 356, and 365 per year, about one per day, against 1143, 686, and 447 attempts. Split by event, first restarts after sunrise carried 41-83 % of the loss and aborted attempts 0.7-18 %. Because a window that opens at the evening stop can close at a later attempt, a second split, chosen after this result, separates windows spanning the night, which carried 72-99 %. The daily depressurized stop, not intra-day restarting, therefore sets the loss.

Changing controller parameters can affect number of aborts but not this statement. With a debounce time of 5 and 15 min the values were 11.37 % and 10.17 % respectively for nominal full shutdown at Cabauw. Using the abort-hold variant the value was 12.07 %, all far above 1 %. Nominal aborts with 1-min debounce would occur 808 times per year at Cabauw using full shutdown nominal after 1-min dip.

**E. Hourly Input Hides Restart Events**

Hourly input undercounts restart attempts and lowers λ_SU, so the event model raises the resolution bias on delivered hydrogen (Fig. 5). Under full shutdown, 60-min block means suppressed 67, 45, and 18 % of the attempts, while completed restarts changed little (ratio 0.96-1.00); the undercount therefore falls mainly on aborted attempts. Delivered hydrogen consequently rose by 10.3 % at Cabauw and 2.4 % at Carpentras and stayed nearly unchanged at Gobabeb.

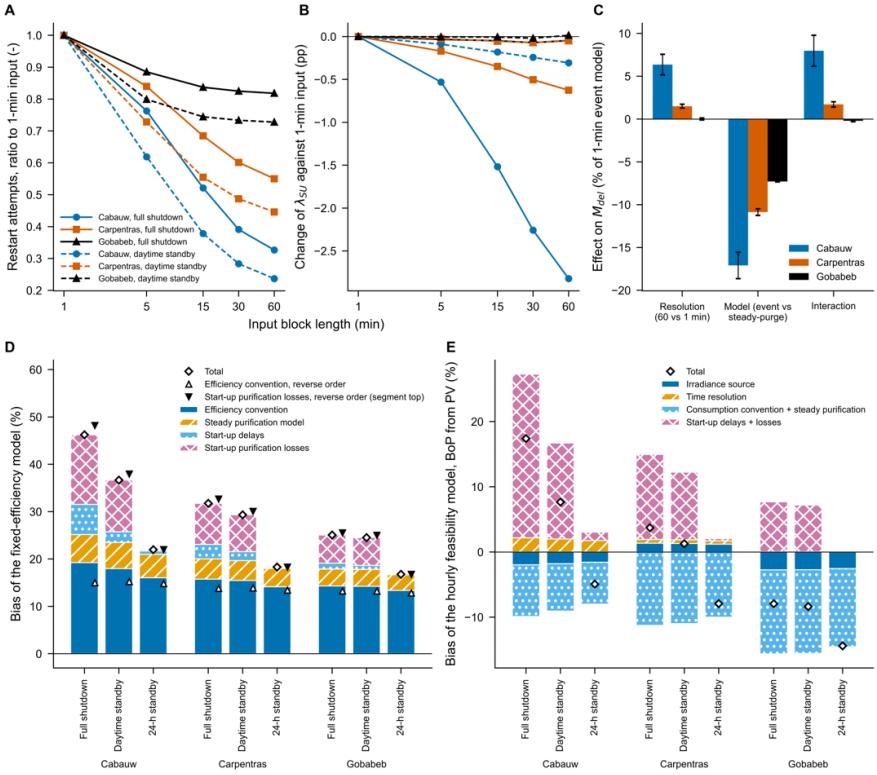


**Figure 5.** Effect of input resolution and of conventional models on delivered hydrogen. (A) Ratio of restart attempts to the 1-min value and (B) change of nominal λ_SU against the 1-min value, by input block length. (C) Main effects and interaction of the 2 × 2 factorial on delivered hydrogen under full shutdown, in percent of the 1-min event model; bars show site means and whiskers the standard deviation over site-years. (D) Bias of the fixed-efficiency model by term at nominal parameters, forward order, with reverse-order markers for the two largest terms. (E) Bias of the hourly feasibility model by term against an event model that draws BoP from PV.

Using the factorial design the model choice can be distinguished from the input choice (Fig. 5C). At all sites the model choice was more important than input choice. At Cabauw and Carpentras they had some effect on one another. For example the 60 vs. 1 min input choice only had an effect of +2.4 % using the steady purge model at Cabauw. Short dips will be hidden when using coarse inputs so there are less attempts and less hydrogen lost to venting. With the steady model there is no term to hide short dips.

At the clear-sky sites hourly input instead gave slightly less hydrogen than 5-min input. At a PV ratio of 1.0 and fixed efficiency the difference was −0.36 and −0.27 % at Carpentras and Gobabeb, against −0.39 and −0.27 % from the P_min threshold alone. Block means conserve energy, so the sign is deterministic: an hour straddling sunrise or sunset with a mean below P_min discards all its energy. Coarse input also saves no computation. The 255 full-year runs took a median of 0.19 s each (range 0.12-1.01 s) on a 16-thread laptop with 12 single-process runs in parallel, independent of block length. Wall times are single measurements that vary with machine load, and 12 of the 13 runs above 0.5 s belonged to one policy and input configuration.

**F. Conventional Models Overestimate Delivered Hydrogen**

All of the models that did not account for restart losses overestimate delivered hydrogen for the 90 % interval using full shutdown, except for 2 cases depending on the site (Table IV). Models using a fixed efficiency, steady purge and delay on startup and the efficiency curve on curves 1 and 2 have a positive value on the 5th percentile, whereas curve 3 changes sign with the site. The hourly feasibility model will underestimate delivered hydrogen compared to nominal, by the most at Gobabeb. It will overestimate delivered hydrogen compared to the BoP taken from PV model at Cabauw and Carpentras (Fig. 5E). Both conventions are presented, and no average over sites is taken.

**Table 4.** Bias β_b of delivered hydrogen under full shutdown (%): P5 to P95 (P50), pooled over five seeds and site-years

| Baseline | Type | Cabauw | Carpentras | Gobabeb |
|---|---|---|---|---|
| Fixed-efficiency | Classical | 35.4-62.3 (46.3) | 25.1-35.3 (29.5) | 20.3-25.8 (22.6) |
| Hourly feasibility | Engineering practice | −9.4 to 8.5 (−2.2) | −15.3 to −8.3 (−12.2) | −26.0 to −17.3 (−19.9) |
| Steady-purge | Steady purification | 12.9-36.7 (22.5) | 6.3-15.6 (10.3) | 3.2-8.1 (5.3) |
| Efficiency-curve, curve 1 | Efficiency curves | 32.2-65.7 (45.7) | 20.7-32.9 (26.0) | 15.5-21.3 (18.0) |
| Efficiency-curve, curve 2 | Efficiency curves | 19.1-49.9 (31.5) | 6.9-17.8 (11.6) | 1.3-6.4 (3.5) |
| Efficiency-curve, curve 3 | Efficiency curves | 12.5-41.9 (24.5) | 0.0-10.3 (4.5) | −5.8 to −1.0 (−3.7) |
| Start-up-delay | Dynamic start-up, no purification | 18.7-38.3 (26.9) | 11.5-19.4 (14.9) | 8.3-12.9 (10.3) |

Note: Efficiency-curve delivered mass is at nominal, so its interval comes from the event-model denominator only; this model carries perfect foresight, with a dispatch part of 1.6, 0.6, and 0.2 pp on curve 1. Hourly feasibility intervals use the nominal auxiliary convention. Intervals for the other stop policies are part of the data available on request.

Journal of Kyzylorda Scholarly Review
P-ISSN:3006-0265 | E-ISSN:3007-4681
https://bulletin.ouk.kz/index.php/bulletin/index

The bias for the fixed efficiency model has components that vary in type (Fig. 5D). Start up losses account for 14.7 pp out of 46.2 % at Cabauw. This is second to the efficiency convention with 19.3 pp. All locations show the same rank, and the dispatch term is always 0. Order at Cabauw shows the efficiency convention as 15.0 pp and start up loss at 16.7 pp when reversed. Standby of 24-h reduces the bias to 16.8-22.0 % with the majority from the efficiency convention and steady purification. The efficiency term is thus due to the difference between 75 % LHV and the model used for the stack. Start up terms are the additions made in this work.

The steady term is sensitive to its source. Replacing s(L) by the constant shares of Table II raises delivered hydrogen by 3.1-4.7 %, so the steady-purge model inherits a term from a 10-cell laboratory unit. Nominal β lies near or below the median at Cabauw, where nominal P_min is the lower range bound, and above it at the other sites.

**G. GAS INVENTORY DOMINATES THE UNCERTAINTY**

Gas inventory ranked first for λ_SU in all nine sets, with total index 0.45-0.71 (Fig. 6). PV sizing followed at 0.18-0.41, labeled design, and operating pressure at 0.09-0.15, while purge time, blow-down time, thermal, and oxygen factors stayed below 0.1. First-order indices summed to 0.96, so interactions are small, and standby power has no effect on λ_SU by construction. For the bias of the fixed-efficiency and steady-purge models, inventory, PV sizing, pressure, and P_min reach at least 0.1 in part of the sets. Stop policy is a scenario axis, not a Sobol factor, so its weight appears in Table III instead.

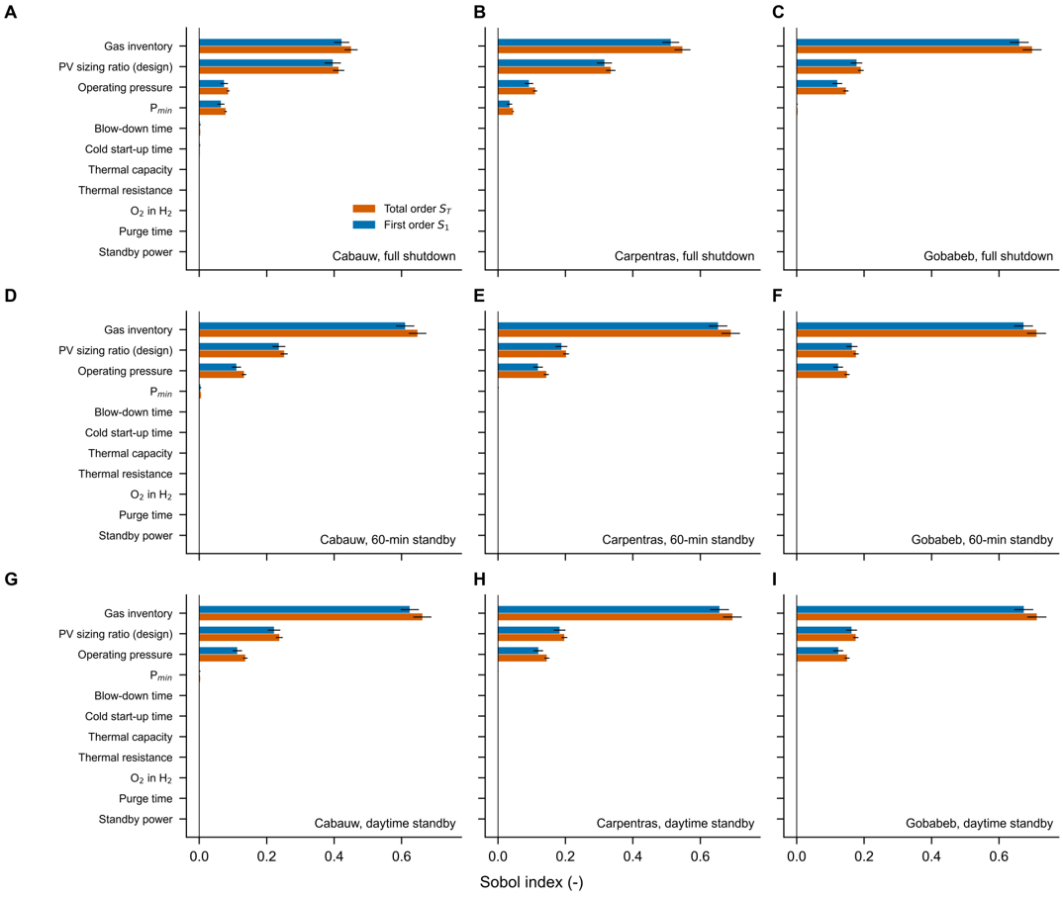


**Figure 6.** Sobol indices of λ_SU at reference years, pooled five-seed estimator. Rows: full shutdown, 60-min standby, and daytime standby; columns: Cabauw, Carpentras, and Gobabeb. Bars show first-order and total indices, and whiskers the 95 % bootstrap half-width.

Journal of Kyzylorda Scholarly Review
P-ISSN:3006-0265 | E-ISSN:3007-4681
https://bulletin.ouk.kz/index.php/bulletin/index

Because inventory carries the largest share of the variance, the result can be rescaled to a given plant. Slopes were 11.6, 7.9, and 5.9 pp per min/bar across the PEM inventory levels, over which (4) reproduced λ_SU under full shutdown within −12.8 to +13.6 %, so a plant can insert its own inventory. Eq. (4) does not apply to standby policies, however: since a hot restart has no blow-down, it overestimates daytime standby by about 100 %.

**H. Hot Standby Trades Standby Energy For Retained Inventory**

Standby with less time recovers some of what was gained with a 24-h standby, at an energy cost dependent on the location (Fig. 7). Using a time of 120 minutes recovered 35, 16 and 6 % of the 24-h standby gain within the modeled mechanisms. This is because a limited standby time covers the stops during the day, whereas the larger term is stopping overnight.

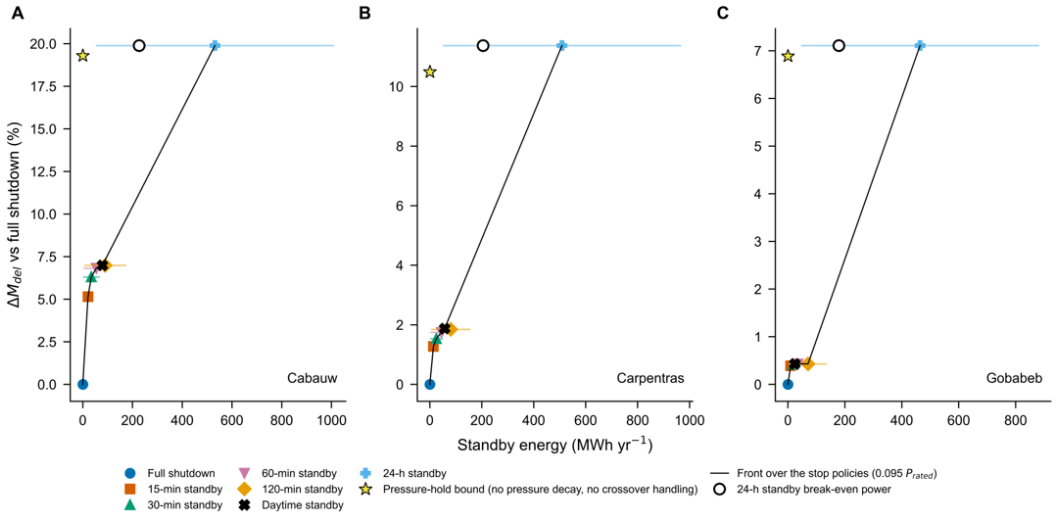


**Figure 7**. Delivered hydrogen gain over full shutdown against standby energy at (A) Cabauw, (B) Carpentras, and (C) Gobabeb. Markers show policies at 0.095 P_rated, and horizontal lines span 0.01-0.18 P_rated. The line is the front over the stop policies, the open circle the break-even standby power of 24-h standby, and the star the pressure-hold bound.

At nominal standby power, 60-min standby costs 35.9, 71.1, and 165.8 kWh of standby energy per kg gained, and 24-h standby 118.9-129.1 kWh/kg, above the stack value of about 50 kWh/kg. Break-even for 24-h standby lies at 0.037-0.040 P_rated. Delivered specific energy with a constant BoP share [30] shows the same trade-off. At 0.01 P_rated, 24-h standby stays below full shutdown at every site, whereas at nominal standby power it exceeds it, with 83.1 against 71.5 kWh/kg at Cabauw. The measured standby of 38-45 kW on a 250 kW plant [26] lies at the high end of this range, where 24-h standby raises delivered hydrogen at a higher delivered specific energy than full shutdown.

The pressure-hold bound attributes 97, 92 and 97 % of the gain from the 24-h standby to retained inventory and the remainder to retained heat. This is only an attribution, for the bounding case of Section III-A. Both standby results hold within the modeled mechanisms.

**I. Conditions Of The Conclusion**

The main conclusion that venting policies carry a material restart loss is true under the stated conditions. But there is one named corner of the parameter space that it does not apply to. On the deterministic grid there were 36 of 324 site, policy and parameter cells that fell under 1 %. These all had an inventory of 0.120 min/bar and used washout times that were not sourced and at most 3.25 rated-minutes. For any washout of at least 6.5 rated-minutes no site-year fell under 1.46 %. No site-year fell under 1.43 % when using the nominal inventory, including 12 bar. The 1 % level would need an average of 2.5-4.6 rated-minutes per completed restart, which is lower than any of the full-shutdown means in Table III. These grid results are a screen, not a class.

Alkaline-derived ends act only upward. An inventory of 3.178 min/bar from a 2 $Nm^3/h$ pilot gave 35.4 % at Cabauw and 20.3 % at Gobabeb under full shutdown, and a washout of 100 rated-minutes, set from the 100 min an alkaline system needed to meet the nitrogen limit after a cold start [41], gave 24.8-41.3 % at the nominal inventory. Neither is a PEM result. Drawing BoP from the PV bus with a constant share raised λ_SU by 0.65-1.94 pp and lowered delivered hydrogen by 11.9-16.7 %. Adding incidence-angle loss with a DC/DC efficiency of 0.96 raised λ_SU by 0.21-0.59 pp and lowered delivered hydrogen by 4.1-5.4 %.

Dryer regeneration state lies outside λ_SU, and the bed model bounds it at up to about three quarters of the median per-restart loss under full shutdown. Re-pressurization takes 0.006 kg per restart, which is non-influential, and one extra regeneration purge takes 0.30-0.50 kg. Measured data fix the mechanism: the laboratory bed reached a minimum dew point of −72.2 °C after 2.5 h of regeneration but only −48.9 °C after 1.5 h, against the −65.5 °C breakpoint [19]. At plant level, an assumed bed sequence with countercurrent regeneration gave no off-specification gas at 2.5 h and 5.3-6.1 kg per restart at 1.5 h over the grid band (Richardson extrapolation 4.6-5.1 kg). These values are bounds from the bed model tested in Fig. 2, not results. The off-specification gas appears at the end of the adsorption step, a capacity shortfall under fixed-time switching, so a humidity-controlled switch would replace it by an earlier regeneration within the extra-purge bound. The feed-direction purge case is not used as a bound, because the measurements contradict the model in that configuration.

**J. Comparison With Related Works**

No better-or-worse ranking applies to λ_SU, because none of the five works reports a restart-loss quantity; they overlap with this study on parts of the chain only (Table V). Renau et al. [15] shares the steady purge term, re-run here as the steady-purge model, and differs in scope, since it uses hourly input, a laboratory stack, and no restart events. Xu et al. [8] and Dong et al. [7] answer a neighboring question on alkaline technology, namely how to shorten a cold start. They are complementary rather than comparable, although the venting that Dong et al. [7] mention is the term quantified here for PEM.

Virah-Sawmy et al. [11] overlaps on two terms, with the same definitions and the code that reproduced its tables. The direction of the efficiency term agrees at every site. At its ratio of 1.0 the term was −3.3, −9.9, and −13.2 % at Cabauw, −4.0, −12.1, and −16.1 % at Carpentras, and −4.4, −13.2, and −17.7 % at Gobabeb for curves 1, 2, and 3. Gobabeb lies inside the reported ranges of Table V, Carpentras below them in size by 0.2-0.6 pp, and Cabauw by 0.9-3.5 pp, whereas at 0.75 Cabauw lies inside and Gobabeb beyond by 0.4-2.2 pp. The ratio shares a value but not a base, rated farm capacity there and PV DC peak here, so the cause of these site differences remains unassigned. Capacity factor does not order the term, since the farms of that study give −4.6 % at 17 %, −4.4 % at 19 %, and −5.1 % at 24 %. The share of 5-min energy above 0.3 P_cap does place the nine plant values and the three farm values in the same sequence as the term. This ordering remains descriptive. For curve 1 the algebraic estimate of the upper curve segment stays below the term in size by up to 0.052 pp at the plant and 0.17 pp at the farms, beyond the 0.04 pp tolerance at Cabauw at a ratio of 1.0. Curves 2 and 3 add no independent test, because the three curves scale as 1:3:4.

Timestep at a ratio of 0.75 was between +0.6 and +1.3 % at Cabauw which falls within the given interval. Carpentras gave results between −0.1 and +0.2 % while Gobabeb was between −0.2 and −0.1 %. This is due to the threshold effect of Section IV-E. When fully shutting down at the plants ratio delivered hydrogen changed by +6.61, +1.21, and −0.46 % of the 5-min value. At Cabauw this exceeds the given interval as there is an energy penalty when venting is not used. Almpantis et al. [12] is partly comparable. The metric class is equal, but no site-specific values could be found for Gobabeb, and the definition of their reconfiguration events was not available. Compared to these papers this work has full years of measured 1-min data for three locations, a deliverable metric and decision rules fixed before the annual runs. Its evidence base is narrower. Renau et al. [15] compared against plant data (15.65 % of mean

flow). Dong et al. [7] had data from a 250 kW system and Xu et al. [8] ran a hardware in the loop test. No system-level measurement supports the present restart losses.

**Table 5.** Comparison With Related Works: Scope, Overlaps, And Differences

| Ref | Year | Method | Data/System | Metrics | Values | Reported/Re-run | Directly comparable? | Limitation |
|---|---|---|---|---|---|---|---|---|
| Renau et al. [15] | 2025 | Steady polynomial PEM model, load-dependent PSA purge loss | 10-cell 50 cm² PEM, hourly PVGIS, European sites | Purge share, BoP share, LCOH | Purge 26.7 to 3.9 % | Purge term re-run as the steady-purge model: $\beta$ full shutdown 21.1/11.7/7.2 % (interval in Table IV); 24-h standby 1.0/0.3/0.07 % | Partly: steady purge term only; annual output no (laboratory stack, hourly input, other sites) | No restart events; hourly; laboratory scale |
| Xu et al. [8] | 2025 | Start-up-aware AWE control | Multi-unit AWE, PV typical days, hardware-in-the-loop | Cold-start time, H2, LCOH | −5.68/−38.94 %; +45.37/+11.38 %; −29.83/−10.09 % | Reported | No: controller objective, other technology, abstract level | Purification not treated |
| Virah-Sawmy et al. [11] | 2024 | Mixed-integer dispatch, efficiency curves, 5-60 min | 3 solar + 3 wind farms, 2022 market data | H2 difference fixed vs variable efficiency; 60 vs 5 min | Curves 1/2/3: −4.2 to −5.1/−12.5 to −14.9/−16.7 to −19.9 %; timestep 0.2-2 % | Re-run: 12 of 12, largest error 5.2 %; plant terms as in the text | Yes for two terms; consistency check; ratio on a different base | No purification or BoP |
| Almpantis et al. [12] | 2026 | 1-min PV-PEM co-simulation, 7 architectures | 4 sites, 1.5 kW stack, summer windows | Hourly minus minute H2, reconfiguration events suppressed | 4.2-6.8 % (Lyngby); about 96 % (Lyngby), 63 % (Navarra) | Reported; computed here: full shutdown/day time standby/24-h standby Cabauw +4.6/+2.5/+2.6, Carpentras | Partly: metric class equal; no same-site value; definition unavailable; stack scale | No purification; summer only |

**Table 5.** Comparison With Related Works: Scope, Overlaps, And Differences

| Ref | Year | Method | Data/System | Metrics | Values | Reported/Re-run | Directly comparable? | Limitation |
|---|---|---|---|---|---|---|---|---|
| | | | | | | +0.3/−0.1/+0.5, Gobabeb +0.5/+0.1/+0.4 %; suppressed 63-72, 30-38, 20-26 % | differs | |
| Dong et al. [7] | 2026 | Electrochemical-thermal AWE cold-start optimization | 250 kW AWE | Start-up time, energy | −23.12/−6.79 %; −45.90/−43.71 % | Reported | No: single event, controller objective, abstract level | Venting acknowledged, not quantified |
| This work | 2026 | Event-based restart state machine with H2 fate accounting, 1-min annual | 1 MW PEM + 1.5 MWp, 3 sites, 17 site-years | $\lambda_{SU}$, $\tau_{eq}$, $\eta_{del}$, $\beta$, restart counts, class | Table III, under its stated conditions | Re-run (all) | Metric has no counterpart in the five works | Component-level tests only; passed tests touch non-driving terms; inventory contested; washout fixed; dryer regeneration state unresolved; pressure-hold case bounding; no end-to-end validation; PEM only |

Note: LCOH is the levelized cost of hydrogen; site triples follow the order of Section III-B.

**Limitations**

The work presented here sits at the evidence level of numerical feasibility plus component-level tests. There was no measured per-restart hydrogen balance on a PEM plant. Tests that were within tolerance only touch terms without influence on the restart loss. Blow-down and washout had no test that fell within tolerance. These restart losses are therefore conditional model results of the stated procedures. The gas inventory and procedures for washout and blow-down are taken from limited PEM information and one alkaline pilot. This sets the width of the reported intervals. The results are applicable to one 1 MW PEM restart unit at three sites. No storage or degradation is included in the loss calculation. Dryer regeneration state and standing loss while in standby are not included in the modeled loss.

**Conclusion**

The stop policies that vent the gas inventory and purge with nitrogen withheld a material share of stack hydrogen from delivery at all locations. The daily depressurized stop set the size of the restart loss. Gas inventory ranked first among the sampled factors. Hot standby decreased the modeled loss but added to the energy spent during standby. Based on this component-

level evidence, yield assessments should treat restart venting as an event. A steady purification model overestimated delivered hydrogen under full shutdown. Future work should measure a per-restart hydrogen balance on a megawatt PEM plant, including gas inventory and dryer regeneration state.

**Data and Code Availability**

Irradiance data are available from the Baseline Surface Radiation Network through PANGAEA under the BSRN data release conditions. Market data of the Australian National Electricity Market for 2022 are publicly archived by the Australian Energy Market Operator. Hourly PVGIS data are available from the Joint Research Centre of the European Commission. The simulation code and the data supporting the findings of this study are available at [my_project.htm].

**Declarations**

Competing interests: The authors declare that they have no known competing financial interests or personal relationships that could have appeared to influence the work reported in this paper.

Funding: This research did not receive any specific grant from funding agencies in the public, commercial, or not-for-profit sectors.

**References**

[1] E. Kuhnert, K. Mayer, M. Heidinger, C. Rienessel, V. Hacker, and M. Bodner, "Impact of intermittent operation on photovoltaic-PEM electrolyzer systems: A degradation study based on accelerated stress testing," International Journal of Hydrogen Energy, vol. 55, pp. 683–695, 2024, doi: 10.1016/j.ijhydene.2023.11.249.

[2] Hydrogen fuel quality — Product specification, ISO 14687:2025, International Organization for Standardization, 2025.

[3] H. Sayed-Ahmed, Á. I. Toldy, and A. Santasalo-Aarnio, "Dynamic operation of proton exchange membrane electrolyzers—Critical review," Renewable and Sustainable Energy Reviews, vol. 189, Art. no. 113883, 2024, doi: 10.1016/j.rser.2023.113883.

[4] Y. Zheng, C. Huang, J. Tan, S. You, Y. Zong, and C. Træholt, "Off-grid wind/hydrogen systems with multi-electrolyzers: Optimized operational strategies," Energy Conversion and Management, vol. 295, Art. no. 117622, 2023, doi: 10.1016/j.enconman.2023.117622.

[5] F. Superchi, F. Papi, A. Mannelli, F. Balduzzi, F. M. Ferro, and A. Bianchini, "Development of a reliable simulation framework for techno-economic analyses on green hydrogen production from wind farms using alkaline electrolyzers," Renewable Energy, vol. 207, pp. 731–742, 2023, doi: 10.1016/j.renene.2023.03.077.

[6] A. Ibáñez-Rioja et al., "Off-grid solar PV–wind power–battery–water electrolyzer plant: Simultaneous optimization of component capacities and system control," Applied Energy, vol. 345, Art. no. 121277, 2023, doi: 10.1016/j.apenergy.2023.121277.

[7] X.-J. Dong, S.-Y. Hu, J.-N. Shen, and Y.-J. He, "Optimal cold startup for alkaline water electrolysis: An electrochemical-thermal coupled model based multi-objective optimization approach," Energy Conversion and Management, vol. 357, Art. no. 121456, 2026, doi: 10.1016/j.enconman.2026.121456.

[8] H. Xu et al., "Optimization control strategy for photovoltaic/hydrogen system efficiency considering the startup process of alkaline electrolyzers," International Journal of Hydrogen Energy, vol. 106, pp. 65–79, 2025, doi: 10.1016/j.ijhydene.2025.01.462.

[9] E. Rauls, M. Hehemann, R. Keller, F. Scheepers, M. Müller, and D. Stolten, "Favorable start-up behavior of polymer electrolyte membrane water electrolyzers," Applied Energy, vol. 330, Art. no. 120350, 2023, doi: 10.1016/j.apenergy.2022.120350.

[10] A. Stock, F. Superchi, E. Hart, and A. Bianchini, "Impact of sub-hourly wind dynamics on green hydrogen yield and electrolyser lifetime," Applied Energy, vol. 427, Art. no. 128976, 2027, doi: 10.1016/j.apenergy.2026.128976.

[11] D. Virah-Sawmy, F. J. Beck, and B. Sturmberg, "Ignore variability, overestimate hydrogen production – Quantifying the effects of electrolyzer efficiency curves on hydrogen production from renewable energy sources," International Journal of Hydrogen Energy, vol. 72, pp. 49–59, 2024, doi: 10.1016/j.ijhydene.2024.05.360.
[12] D. Almpantis, H. Wöhlert, M. H. Fouladfar, H. Davidsson, and M. Andersson, "Python–Simulink simulation of DC-coupled PV–PEM electrolyzer systems under minute-level solar variability," Solar Energy Advances, vol. 6, Art. no. 100149, 2026, doi: 10.1016/j.seja.2026.100149.
[13] J. Lehmann, A. Wabbes, E. Miguelañez Gonzalez, and S. Scheerlinck, "Levelized cost of hydrogen calculation from off-grid photovoltaic plants using different methods," Solar RRL, vol. 6, no. 5, Art. no. 2100482, 2022, doi: 10.1002/solr.202100482.
[14] P. Vargas-Ferrer, E. Sauma, and F. Jalil-Vega, "Incorporating intra-hour renewable variability into the design of stand-alone electrolytic hydrogen production systems," Applied Energy, vol. 404, Art. no. 126982, 2026, doi: 10.1016/j.apenergy.2025.126982.
[15] J. Renau et al., "Solar-powered hydrogen production: Modelling PEM electrolyser systems for optimal integration with solar energy," International Journal of Hydrogen Energy, vol. 189, Art. no. 152126, 2025, doi: 10.1016/j.ijhydene.2025.152126.
[16] S.-L. Steinacker, P. Renze, M. Winter, G. Schullerus, and T. Zenner, "Efficiency analysis based on a balance of plant model for a modular electrolysis system," in 2025 14th International Conference on Renewable Energy Research and Applications (ICRERA), 2025, pp. 659–664, doi: 10.1109/icrera66237.2025.11283834.
[17] E. Crespi, G. Guandalini, L. Mastropasqua, S. Campanari, and J. Brouwer, "Experimental and theoretical evaluation of a 60 kW PEM electrolysis system for flexible dynamic operation," Energy Conversion and Management, vol. 277, Art. no. 116622, 2023, doi: 10.1016/j.enconman.2022.116622.
[18] K. Koike et al., "High-efficiency hydrogen dehumidification in polymer electrolyte membrane water electrolysis (PEMWE) by twin-membrane dryer system," International Journal of Hydrogen Energy, vol. 272, Art. no. 157391, 2026, doi: 10.1016/j.ijhydene.2026.157391.
[19] T. M. R. Santos, J. M. Sousa, F. Relvas, and A. Mendes, "High-performing vacuum-pressure swing adsorption unit for drying hydrogen from water electrolysis," Industrial & Engineering Chemistry Research, vol. 65, no. 32, pp. 17315–17332, 2026, doi: 10.1021/acs.iecr.6c00750.
[20] T. Kim, Y. Song, J. Kang, S. K. Kim, and S. Kim, "A review of recent advances in hydrogen purification for selective removal of oxygen: Deoxo catalysts and reactor systems," International Journal of Hydrogen Energy, vol. 47, no. 59, pp. 24817–24834, 2022, doi: 10.1016/j.ijhydene.2022.05.221.
[21] T. Kim, P. Balla, D. Shin, and S. Kim, "A comparison of γ-Al2O3-supported deoxo catalysts for the selective removal of oxygen from high-concentration hydrogen streams," International Journal of Hydrogen Energy, vol. 51, pp. 396–409, 2024, doi: 10.1016/j.ijhydene.2023.06.227.
[22] S. Kwon, S. Eom, and G. Choi, "Effects of operating conditions on the oxygen removal performance of the deoxo chamber in the water electrolysis system," Energies, vol. 16, no. 18, Art. no. 6685, 2023, doi: 10.3390/en16186685.
[23] S. Hu et al., "Study on the synergistic regulation strategy of load range and electrolysis efficiency of 250 kW alkaline electrolysis system under high-dynamic operation conditions," eTransportation, vol. 19, Art. no. 100304, 2024, doi: 10.1016/j.etran.2023.100304.
[24] S. Oikonomidis, M. Ramdin, O. A. Moultos, A. Bos, T. J. H. Vlugt, and A. Rahbari, "Transient modelling of a multi-cell alkaline electrolyzer for gas crossover and safe system operation," International Journal of Hydrogen Energy, vol. 48, no. 88, pp. 34210–34228, 2023, doi: 10.1016/j.ijhydene.2023.05.184.

[25] H. Zhang et al., "Modeling and validation of hydrogen-oxygen impurity in alkaline electrolyzers under multiple operational states for hydrogen-based microgrid scheduling," Applied Energy, vol. 427, Art. no. 128894, 2027, doi: 10.1016/j.apenergy.2026.128894.
[26] M. Persson, D. Mignard, and D. Hogg, "Insights on performance and an improved model for full scale electrolysers based on plant data for design and operation of hydrogen production," International Journal of Hydrogen Energy, vol. 45, no. 56, pp. 31396–31409, 2020, doi: 10.1016/j.ijhydene.2020.08.255.
[27] L. Bonaccorsi et al., "Operational analysis of a pilot-scale plant for hydrogen production via an electrolyser powered by a photovoltaic system," Energies, vol. 18, no. 15, Art. no. 3949, 2025, doi: 10.3390/en18153949.
[28] C. Aijun, P. Jun, Z. Hang, F. Keying, and L. Xubin, "Experimental investigation of hydrogen production performance of PEM electrolyze," Scientific Reports, vol. 15, no. 1, Art. no. 23230, 2025, doi: 10.1038/s41598-025-06351-9.
[29] B. Flamm, C. Peter, F. N. Büchi, and J. Lygeros, "Electrolyzer modeling and real-time control for optimized production of hydrogen gas," Applied Energy, vol. 281, Art. no. 116031, 2021, doi: 10.1016/j.apenergy.2020.116031.
[30] G. Liu et al., "Experimental study on dynamic performance of a 50 kW PEM water electrolysis system for hydrogen production," Energies, vol. 19, no. 16, Art. no. 3844, 2026, doi: 10.3390/en19163844.
[31] M. Pfennig, B. Schiffer, and T. Clees, "Thermodynamical and electrochemical model of a PEM electrolyzer plant in the megawatt range with a literature analysis of the fitting parameters," International Journal of Hydrogen Energy, vol. 104, pp. 567–583, 2025, doi: 10.1016/j.ijhydene.2024.04.335.
[32] A. Driemel et al., "Baseline Surface Radiation Network (BSRN): Structure and data description (1992–2017)," Earth System Science Data, vol. 10, no. 3, pp. 1491–1501, 2018, doi: 10.5194/essd-10-1491-2018.
[33] B. Haurwitz, "Insolation in relation to cloudiness and cloud density," Journal of Meteorology, vol. 2, no. 3, pp. 154–166, 1945, doi: 10.1175/1520-0469(1945)002<0154:IIRTCA>2.0.CO;2.
[34] C. N. Long and Y. Shi, "An automated quality assessment and control algorithm for surface radiation measurements," The Open Atmospheric Science Journal, vol. 2, no. 1, pp. 23–37, 2008, doi: 10.2174/1874282300802010023.
[35] D. G. Erbs, S. A. Klein, and J. A. Duffie, "Estimation of the diffuse radiation fraction for hourly, daily and monthly-average global radiation," Solar Energy, vol. 28, no. 4, pp. 293–302, 1982, doi: 10.1016/0038-092X(82)90302-4.
[36] T. Huld, R. Müller, and A. Gambardella, "A new solar radiation database for estimating PV performance in Europe and Africa," Solar Energy, vol. 86, no. 6, pp. 1803–1815, 2012, doi: 10.1016/j.solener.2012.03.006.
[37] R. Perez, P. Ineichen, R. Seals, J. Michalsky, and R. Stewart, "Modeling daylight availability and irradiance components from direct and global irradiance," Solar Energy, vol. 44, no. 5, pp. 271–289, 1990, doi: 10.1016/0038-092X(90)90055-H.
[38] A. P. Dobos, "PVWatts version 5 manual," National Renewable Energy Laboratory, Tech. Rep. NREL/TP-6A20-62641, 2014, doi: 10.2172/1158421.
[39] Á. Hernández-Gómez, V. Ramirez, and D. Guilbert, "Investigation of PEM electrolyzer modeling: Electrical domain, efficiency, and specific energy consumption," International Journal of Hydrogen Energy, vol. 45, no. 29, pp. 14625–14639, 2020, doi: 10.1016/j.ijhydene.2020.03.195.
[40] T. E. Springer, T. A. Zawodzinski, and S. Gottesfeld, "Polymer electrolyte fuel cell model," Journal of The Electrochemical Society, vol. 138, no. 8, pp. 2334–2342, 1991, doi: 10.1149/1.2085971.



[41] Y. Ligen, H. Vrubel, and H. Girault, "Energy efficient hydrogen drying and purification for fuel cell vehicles," International Journal of Hydrogen Energy, vol. 45, no. 18, pp. 10639–10647, 2020, doi: 10.1016/j.ijhydene.2020.02.035.